



A supraamphiphilic structure [12] based on meroterpenoids and a macrocyclic pillar[5]arene platform has been proposed to overcome the disadvantages of isoprenoid lipids. Pillararenes and well-known macrocyclic compounds such as crown ethers, cyclodextrins, calixarenes, etc. [13] have a tendency to form “host-guest” complexes [14]. At the same time they have a number of attractive characteristics, such as synthetic accessibility, planar chirality, a tubular spatial structure that forms an electron-donor cavity, and, as a consequence, the ability to accommodate fragments of “guests” in the macrocyclic ring [15]. Pillar[n]arenes tend to form complexes with positively charged molecules or molecules containing electron withdrawing groups [16]. Pillar[5]arene complexes with charged pyridinium [17] or imidazolium [18] salts can be built according to the “host-guest” principle. The presence of these properties opens up new opportunities in the formation of vesicles, transmembrane artificial channels, nanoreactors, metal-organic frameworks, liquid crystals, and supramolecular polymers [19].

In this article, we propose and develop a synthetic non-covalent self-assembling system of supramolecular amphiphiles based on “host-guest” complexes of pillar[5]arene and meroterpenoids as a universal drug delivery system (DDS).

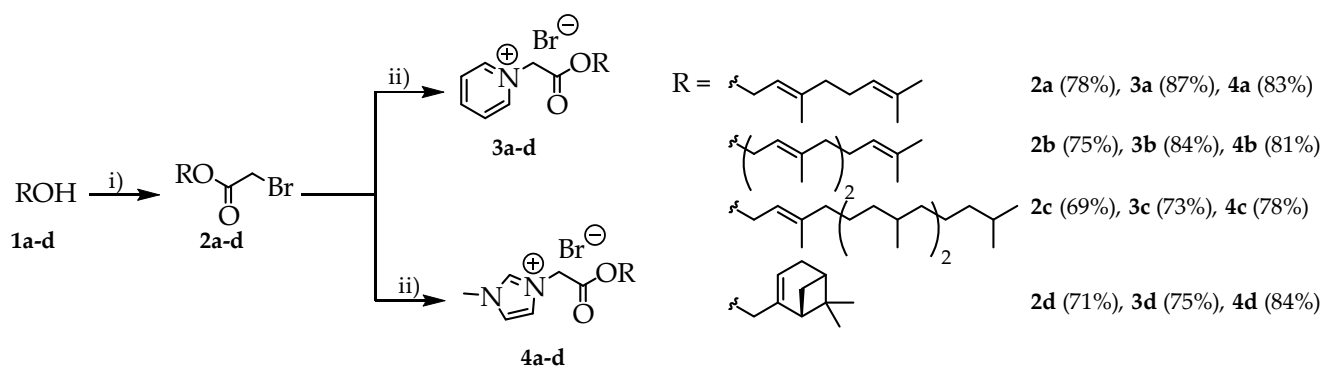
## 2. Results and Discussion

### 2.1. Synthesis of Meroterpenoids Containing Pyridinium and Imidazolium Fragments Based on Terpene Alcohols

It is known [17–21] that compounds containing pyridinium or imidazolium fragments have a tendency to form “host-guest” complexes with pillar[n]arenes. Therefore, we had been aimed to synthesize meroterpenoids containing pyridinium and imidazolium fragments. A supramolecular amphiphiles based on synthesized meroterpenoids and pillar[5]arene can be created by a “host-guest” interaction. The pillar[5]arene can act as a water-soluble component, and the meroterpenoid fragment can act as a lipophilic fragment.

Geraniol, myrtenol (monoterpenols), farnesol (sesquiterpenol) and phytol (diterpenol) were chosen as initial terpenoids for this task. These linear acyclic terpene alcohols have a structure similar to archaeal lipid polyprenols. These terpenols were chosen to create synthetic self-assembling supramolecular analogs of archeosomes on their basis.

At the first stage, we proposed to convert terpene alcohols into terpenyl bromoacetates to create highly reactive alkylating agents (Scheme 1). The compounds **2a,b** have been already described in the literature [22,23], however, methods of their preparation were rather complicated. Therefore, an original technique was developed. *N,N*-Diisopropylethylamine (DIPEA) was used as a base, chloroform as a solvent, the synthesis was carried out at a low (−5 °C) temperature. In this way, terpenyl bromoacetates **2a–d** were obtained with a good yields (Scheme 1).



**Scheme 1.** Reagents and conditions: (i)  $\text{BrCH}_2\text{C(O)Br}$ , DIPEA,  $\text{CHCl}_3$ , −5 °C. (ii) pyridine or *N*-methylimidazole,  $\text{Et}_2\text{O}$ , 20 °C, in case **3c**, **4b,c**:  $\text{Et}_2\text{O}$ , reflux.

The next stage was the synthesis of pyridinium and imidazolium salts based on terpene alcohols. Although compounds **3a,b** and **4b** were described earlier in the liter-

ature [23,24], we developed a more efficient method, which was also applicable to get derivatives of myrtenol and phytol. Diethyl ether was used as a solvent, and the synthesis was carried out at room temperature for 36 h. The products **3a,b,d** after isolation from the reaction mixture were analyzed by  $^1\text{H-NMR}$  spectroscopy. Target products **3a,b,d** and a small impurity of the starting terpenyl bromoacetate were obtained. The products were washed with hexane to remove impurities from the starting compounds. Only the initial phytyl bromoacetate **3c** was observed in the  $^1\text{H-NMR}$  spectrum after removal of the solvent in the case of the phytyl derivative. Apparently, the lipophilic phytyl fragment prevents the reaction due to the formation of aggregates of phytyl bromoacetate in diethyl ether. Then we tried to carry out the reaction of phytyl bromoacetate with pyridine in diethyl ether with heating under reflux. The target product **3c** was obtained using this approach.

The same method was used for obtaining imidazole-containing meroterpenoids **4a–d**. Terpenyl bromoacetates **2a–d** and methylimidazole were used as starting materials. Equimolar amounts of terpenyl bromoacetates and methylimidazole were used for the synthesis of imidazole-containing meroterpenoids (Scheme 1). Thus, it was possible to obtain geranyl and myrtenyl derivatives of methylimidazole. It was necessary to heat the reaction mixtures in the case of farnesyl and phytyl derivatives.

Thus, we have developed a method for the synthesis of the compounds **3a–d** and **4a–d**, based on the alkylation of pyridine and *N*-methylimidazole with terpenyl bromoacetates. The structure of the obtained meroterpenoids were confirmed by  $^1\text{H-}$ ,  $^{13}\text{C-NMR}$  spectroscopy, FT-IR spectroscopy, and high-resolution mass spectrometry (see Supplementary materials, Figures S1–S40).

## 2.2. Self-Assembly of Supramolecular Amphiphiles Based on Pillar[5]Arene and Meroterpenoids Containing Pyridinium and Imidazolium Fragments

Pillar[5]arenes have a tendency to form stable inclusion complexes in solutions with charged pyridinium and imidazolium fragments. In this regard, we proposed to obtain supramolecular amphiphiles in water. Decasubstituted pillar[5]arene **5** was chosen as a water-soluble component (Figure 1), which is a synthetically available model macrocycle [25]. Pyridinium and imidazolium salts **3a–d** and **4a–d** containing a terpenoid fragment were chosen as a lipophilic guest.

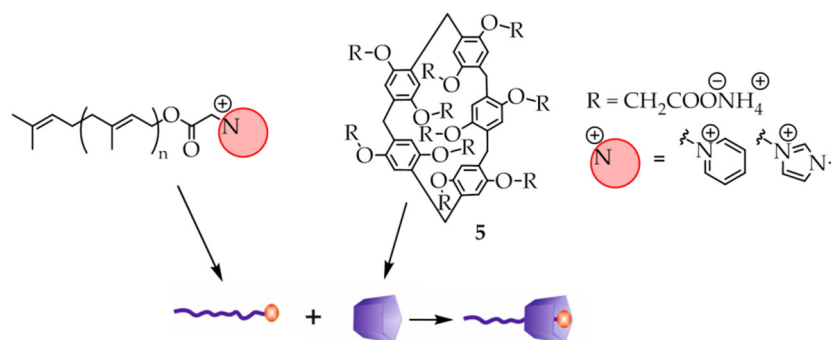


**Figure 1.** The concept of a supramolecular amphiphiles based on pillar[5]arene **5** and amphiphilic meroterpenoids.

The observed upfield shift of proton signals of some fragments in the  $^1\text{H-NMR}$  spectrum indicates inclusion of this fragment into a pillar[5]arene cavity. We have studied the interaction of meroterpenoids **4a–d** with pillar[5]arene **5** in water by  $^1\text{H-NMR}$  spectroscopy, which showed that the charged fragment of imidazolium meroterpenoids **4a–d** is not included in the cavity of the pillar[5]arene, but rather ion replacement occurs. We decided to use methanol as a less polar solvent in order to lower the permittivity and change the type of ionic interaction between the macrocycle and meroterpenoid. As pillar[5]arene **5** is poorly soluble in methanol, it was decided to use a methanol/water mixture in a 2:1 ratio. Figure 2a shows a fragment of the  $^1\text{H-NMR}$  spectrum of mixture of the **4a/5** system

(black) and meroterpenoid **4a** (gray) in a CD<sub>3</sub>OD/D<sub>2</sub>O ( $5 \times 10^{-3}$  M) solution. The analysis of the obtained spectral results showed that the signals of the protons of the imidazolium fragment, methyl (CH<sub>3</sub>N) group, and CH<sub>2</sub>N<sup>+</sup> fragment have an upfield shift. That data indicates the inclusion imidazolium fragments of meroterpenoid **4a** into the cavity of pillar[5]arene. Similar results are observed for myrtenyl derivative **4d** (Figure 2b) and farnesyl derivative **4b**. However, in the case of derivative **4c** in both D<sub>2</sub>O and CD<sub>3</sub>OD/D<sub>2</sub>O, the ion replacement occur in the presence of pillar[5]arene **5**. Apparently, this happens due to the higher lipophilicity of the phytol-based structure. Varying the solvents and temperature did not lead to the formation of the **4c/5** inclusion complex.

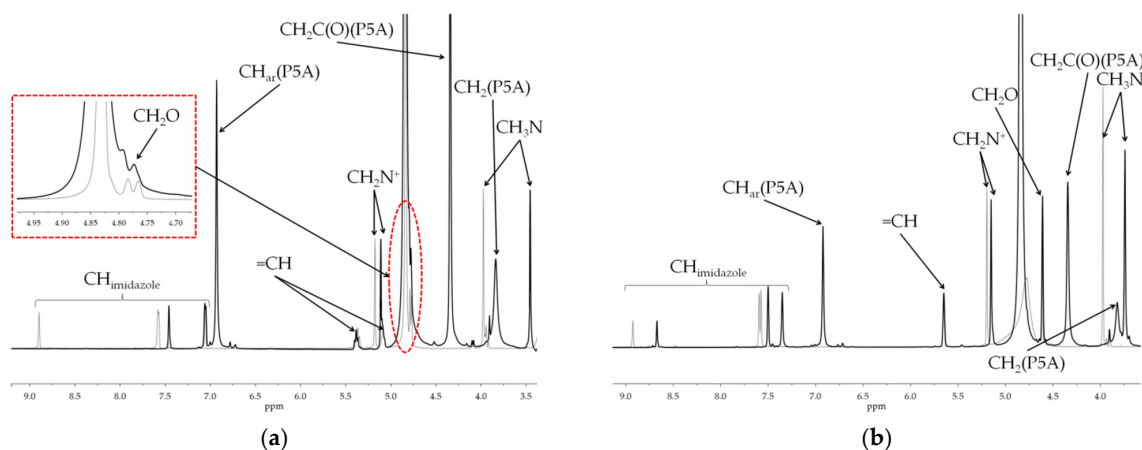


**Figure 2.** Fragments of <sup>1</sup>H-NMR spectrum of systems **4a/5** (a) and **4d/5** (b) (black) and meroterpenoids **4a** and **4d** (gray) in a CD<sub>3</sub>OD/D<sub>2</sub>O mixture ( $5 \times 10^{-3}$  M) at 298 K, 400 MHz.

We have suggested that pyridinium salts, in contrast to imidazolium salts, are more prone to form “host-guest” complexes in water [26]. Figure 3a shows a fragment of the <sup>1</sup>H-NMR spectrum in D<sub>2</sub>O ( $1 \times 10^{-3}$  M) of the **3a/5** system (black) and meroterpenoid **3a** (gray). The signals of the proton of the pyridinium and CH<sub>2</sub>N<sup>+</sup> fragment are shifted in the region of stronger fields by ~0.2 ppm. This data indicates the inclusion of the pyridinium fragment into the cavity of the pillar[5]arene **5** and the formation of an inclusion complex. Similar results (Figure 3b) are observed in the <sup>1</sup>H-NMR spectrum of compound **3b** (a farnesol derivative) in the presence and absence of pillar[5]arene. Thus, pyridinium fragment of the synthesized meroterpenoids **3a–d** inclusion into the cavity of the pillar[5]arene **5** in water and form a supramolecular amphiphile according to the “host-guest” principle.

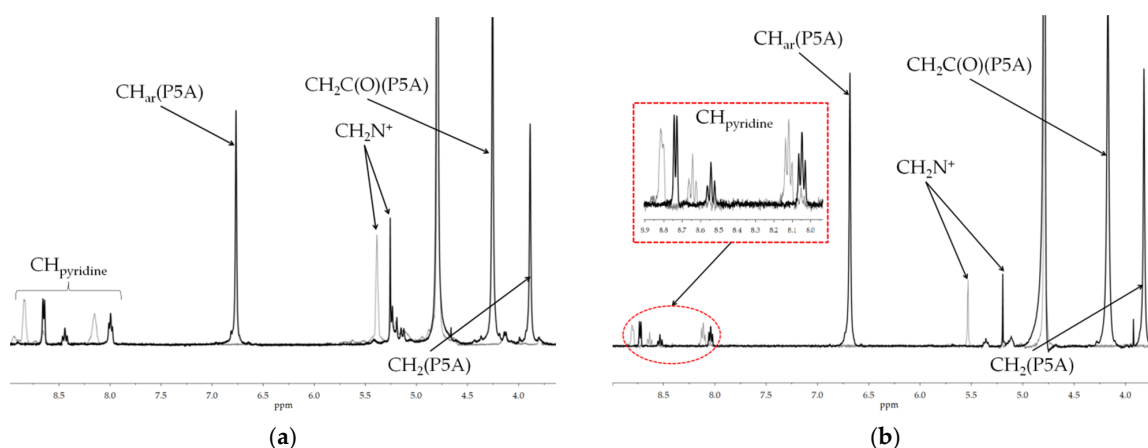


**Figure 3.** Fragments of <sup>1</sup>H-NMR spectra of systems **3a/5** (a) and **3b/5** (b) (black) and meroterpenoids **3a** and **3b** (gray) in D<sub>2</sub>O ( $1 \times 10^{-3}$  M) at 298 K, 400 MHz.

Further, systems **4a/5** in different ratios of components in a methanol/water mixture (2:1) were studied by the dynamic light scattering (DLS) method (Table 1). It was shown that in the presence of pillar[5]arene **5**, the hydrodynamic particle diameter increases from 475 nm to 562 nm. Upon reaching a 5-fold excess of macrocycle **5** in a meroterpenoid/pillar[5]arene mixture, a sharp increase in the hydrodynamic diameter and polydispersity index (PDI) of aggregates occurs. This indicates coagulation of particles. Similar results were obtained when studying the interaction of imidazolium salts **4b** and **4d** with pillar[5]arene **5**. In the case of farnesyl and myrtenyl derivatives **4b,d**, particle coagulation begins at a meroterpenoid/pillar[5]arene ratio of 1:2. Thus, the aggregates retain their diameter and polydispersity index up to a 1:1 ratio, after which coagulation of particles begins.

**Table 1.** Sizes of aggregates (average hydrodynamic diameter) in a methanol/water (2:1) mixture of compounds **4a,b,d** ( $1 \times 10^{-3}$  M) in the presence and in the absence of pillar[5]arene **5**, obtained by the DLS method.

Ratio 4/5	4a		4b		4d	
	d	PDI	d	PDI	d	PDI
–	475 ± 22	0.24	420 ± 19	0.19	521 ± 25	0.17
1:0.1	522 ± 13	0.26	501 ± 21	0.19	607 ± 24	0.22
1:0.2	515 ± 12	0.23	505 ± 13	0.21	635 ± 22	0.20
1:0.5	532 ± 36	0.20	513 ± 29	0.22	645 ± 29	0.28
1:1	562 ± 43	0.26	578 ± 53	0.46	662 ± 31	0.29
1:2	615 ± 36	0.35	915 ± 46	0.65	1606 ± 236	0.56
1:5	1216 ± 267	0.60	925 ± 87	0.61	1701 ± 298	0.69
1:10	1597 ± 312	0.67	997 ± 312	0.69	1698 ± 309	0.70

Then, we studied the aggregation of systems **3a–d/5** and meroterpenoids **3a–d** in water by the DLS method (Table 2). Associates of geranyl and farnesyl derivatives **3a** and **3b** presumably have different structures. This is proven by insignificant changes in the average hydrodynamic diameter of aggregates in the case of geranylpyridinium salt, and significant changes in the average hydrodynamic diameter of aggregates in the case of farnesylpyridinium salt. Aggregates of phytolpyridinium salt **3c** have the same hydrodynamic diameters in the presence and in the absence of pillar[5]arene **5**. Apparently, this is due to the conformational softness of the phytol chain, in which there are fewer double bonds, in contrast to geranyl chain and farnesyl chain.

**Table 2.** Sizes of aggregates (average hydrodynamic diameter) of compounds **3a–d** ( $1 \times 10^{-4}$  M) in water in the presence and in the absence of pillar[5]arene **5**, obtained by the DLS method.

Ratio 3/5	3a		3b		3c		3d	
	d	PDI	d	PDI	d	PDI	d	PDI
–	129 ± 2	0.23	144 ± 4	0.17	208 ± 13	0.30	198 ± 15	0.41
1:0.1	162 ± 2	0.08	208 ± 16	0.14	205 ± 9	0.29	189 ± 24	0.44
1:0.2	164 ± 14	0.14	379 ± 10	0.16	204 ± 7	0.27	234 ± 28	0.42
1:0.5	157 ± 5	0.12	411 ± 12	0.18	209 ± 4	0.31	198 ± 21	0.41
1:1	163 ± 2	0.10	386 ± 10	0.20	202 ± 5	0.27	237 ± 40	0.52
1:2	162 ± 6	0.06	348 ± 13	0.22	207 ± 18	0.29	313 ± 74	0.55
1:5	156 ± 3	0.19	297 ± 6	0.22	205 ± 12	0.29	253 ± 46	0.50
1:10	166 ± 5	0.28	285 ± 27	0.23	203 ± 8	0.29	259 ± 45	0.49

We also measured the zeta-potential of meroterpenoids **3a–d** in the absence and in the presence of pillar[5]arene **5** in various ratios in water (Figure 4). The value of the zeta-potential indicates the stability of the colloidal system. Point 0.0 (Figure 4) on the abscissa axis corresponds to the value of the zeta-potential for the meroterpenoid solution

in the absence of pillar[5]arene. The zeta-potential of the system begins to change sharply when pillar[5]arene is added to the meroterpenoid solution. The dependence reaches a plateau at a molar ratio of 1:1 and zeta-potential values of  $-50$ – $-70$  mV. Negative values of the zeta potential indicate that carboxylate fragments of the pillar[5]arene are located on the surface of the aggregates.

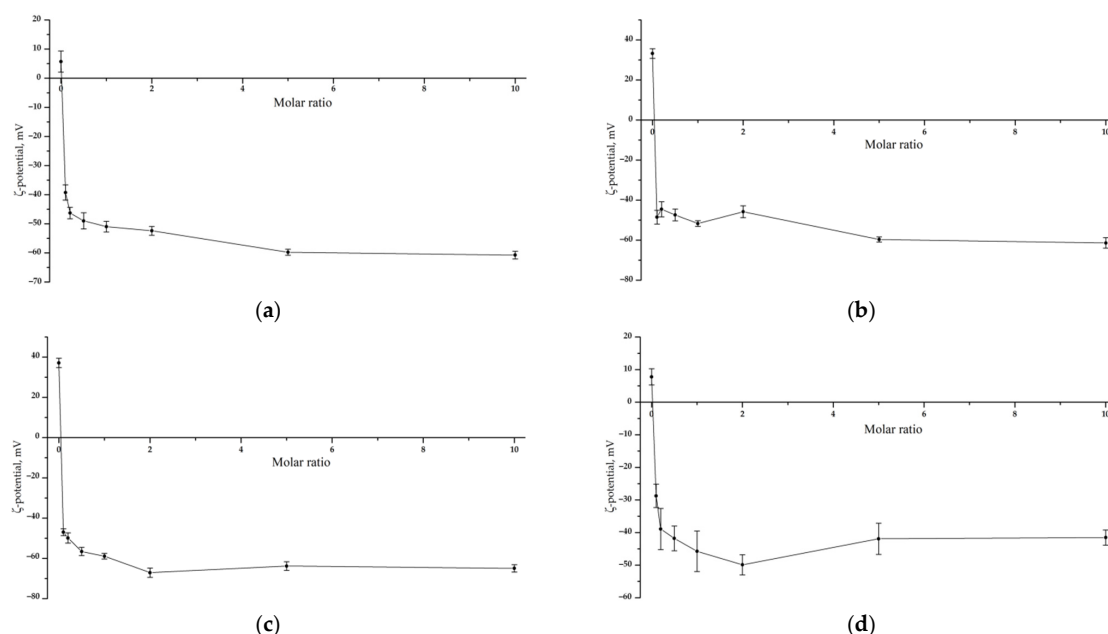


**Figure 4.** Dependences of the zeta-potential on the molar ratio of pillar[5]arene 5/meroterpenoids 3a–d, (a)—5/3a, (b)—5/3b, (c)—5/3c, (d)—5/3d.

Then, the interaction between pillar[5]arene 5 and meroterpenoids 3a,b was studied by UV-vis spectroscopy. A hypochromic effect at the macrocycle wavelength  $\lambda = 295$  nm are observed for systems 3a/5 and 3b/5. Spectrophotometric titration methods were used to determine the binding constants. The absorption spectra of the 3a,b/5 systems were recorded with the concentration of pillar[5]arene 5 ( $1 \times 10^{-5}$  M) remaining constant, and the various concentration of 3a,b ( $1 \times 10^{-6}$ – $1 \times 10^{-5}$  M). The data obtained were processed by BindFit [27]. The association constant of 3a/5 (1:1) was  $8557 \text{ M}^{-1}$  and 3b/5 (1:1) was  $14,900 \text{ M}^{-1}$ . Moreover, the stoichiometry of the complex was confirmed by titration data processed using host-guest ratios of 1:2 and 2:1. However, in this case, the association constants of the complexes were determined with a large error. That confirms the correctness of our chosen 1:1 model (see Supplementary materials Figures S41–S43). These data confirm the correctness of our chosen 1:1 stoichiometry.

Thus, ionic substitution occurs in aqueous solutions of derivatives 4a,b,d in the presence of pillar[5]arene. Supramolecular amphiphiles 4a,b,d/5 are formed in a water-methanol mixture. In the case of phytol derivative 4c, ion substitution occurs both in water and in a water-methanol mixture. It was also shown that the pyridinium fragment of the synthesized meroterpenoids 3a–d are include into the pillar[5]arene cavity in water to form the supramolecular amphiphile 3a–d/5 according to the “host-guest” principle. BindFit calculations showed that the stoichiometry of inclusion complexes 3a,b/5 was 1:1.

### 2.3. Membranotropic Activity of Supramolecular Amphiphiles Based on Pillar[5]Arene and Meroterpenoids Containing Pyridinium and Imidazolium Fragments

Next, the interaction of supramolecular amphiphiles with model dipalmitoylphosphatidylcholine (DPPC) vesicles at pH = 7.4 was studied. We used the turbidimetry method to determine the temperature ( $T_m$ ) of the phase transition of DPPC vesicles. The binding of amphiphilic compounds by the lipid bilayer is accompanied by a change in the packing

density of lipids. The phase transition temperature  $T_m$  (gel—liquid crystals) is a sensitive indicator of the state of lipid molecules in the bilayer.  $T_m$  was determined by measuring the turbidity of the water lipid dispersion with increasing temperature [28]. This method is convenient because it does not depend on the influence of scattering particles, because the phase transition is recorded as a sharp decrease in absorption within a certain narrow temperature range, typical of the selected lipid.

It was shown that pyridinium salt **3a** leads to a linear decrease in the phase transition temperature of lipid vesicles depending on the concentration of the substance (Figure 5a, red graph). Pillar[5]arene **5** does not lead to a change in the phase transition temperature of the vesicles. Similar studies for the system **3a/5** showed that in this case there is no noticeable decrease in the temperature ( $T_m$ ) of the phase transition of vesicles (Figure 5a, blue dots). The imidazolium derivative of geraniol **4a** leads to a linear decrease in the phase transition temperature of the vesicles (Figure 5b). However, the system **4a/5** does not lead to changes in the phase transition temperature ( $T_m$ ) of vesicles (Figure 5b). It means the absence of interaction of the supramolecular amphiphile **4a/5** with the model phospholipid membrane. The situation is similar for the derivatives of myrtenol—**3d** and **4d**. They lead to a linear decrease in the phase transition temperature (Figure 6, red graphs). Systems **3d/5** and **4d/5** does not lead to the decrease of phase transition temperature ( $T_m$ ) of the lipid vesicles (Figure 6, blue dots). It was also shown that meroterpenoids based on farnesol and phytol **3b,c** and **4b,c** lead to the solubilization of phospholipid vesicles above the molar ratio of substance/lipid of 0.1. However, supramolecular amphiphiles **3b/5**, **3c/5** and **4b/5** does not lead to changes in the phase transition temperature ( $T_m$ ) of lipid vesicles.

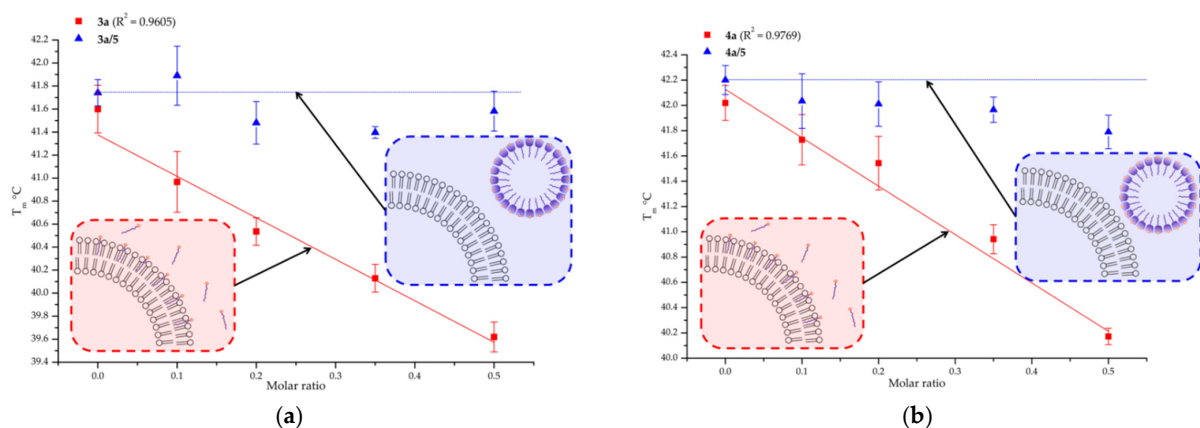


**Figure 5.** Dependences of the lipid phase transition temperature  $T_m$  (DPPC) on the amount of **3a** (a) **4a** (b) (red) and systems **3a/5** (a) **4a/5** (b) (blue) at pH = 7.4.

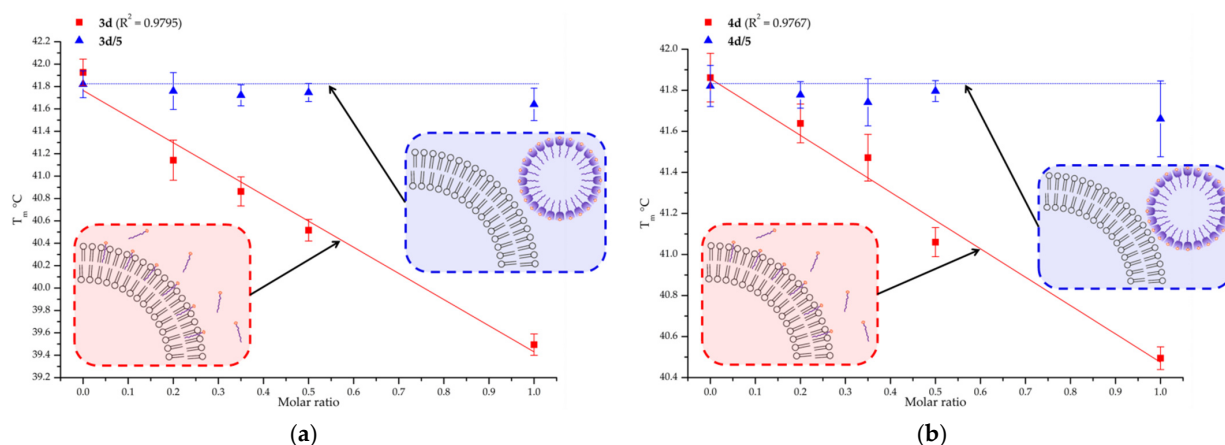


**Figure 6.** Dependences of the lipid phase transition temperature  $T_m$  (DPPC) on the amount of **3d** (a) **4d** (b) (red) and systems **3d/5** (a) **4d/5** (b) (blue) at pH = 7.4.

It can be concluded that meroterpenoids containing pyridinium fragments **3a,d** cause a greater decrease in temperature, in contrast to analogous imidazolium derivatives **4a,d**. Apparently, this is due to the higher polarity of the imidazolium fragment. It can also be concluded that acyclic monoterpenoid derivatives (with a geranyl fragment) **3a** and **4a** cause a greater decrease in the phase transition temperature ( $T_m$ ), in contrast to bicyclic monoterpenoids (with a myrtenyl fragment) **3d** and **4d**. This is most likely due to the size of the lipophilic substituent. The linear geranyl fragment can be more efficiently embedding into lipid bilayer, in contrast to the bicyclic myrtenyl fragment. Thus, based on the turbidimetric data, it follows that meroterpenoids **3a,d** and **4a,d** are embedded into lipid bilayers. At the same time, all systems of supramolecular amphiphiles **3a/5** and **4a/5** did not show any interaction with the phospholipid vesicle under these conditions, which makes it possible to use these associates as targeted drug delivery systems.

The lack of interaction between supramolecular amphiphiles and the phospholipid membrane is explained by the stability of the aggregates that form supramolecular amphiphiles. It has been suggested that a decrease in pH will disrupt the stability of the supramolecular amphiphiles aggregates and influence their interaction with the phospholipid membrane. The extracellular pH of tumor cells is known to be acidic [29,30]. Therefore, the phase transition temperatures of lipid vesicles in the presence of compound **3a** and the **3a/5** system at pH 4.1 were measured. The obtained dependence is presented in Figure 7. The supramolecular system of amphiphiles **3a/5** interacts with the phospholipid membrane at pH 4.1 (the blue graph on Figure 7). The linear nature of the dependence of the phase transition temperature ( $T_m$ ) of lipid vesicles indicates that the bilayer structure is not destroyed during interaction. Thus, it was shown that supramolecular amphiphiles interact with a lipid bilayer, only under certain conditions, with a possible pH-control.

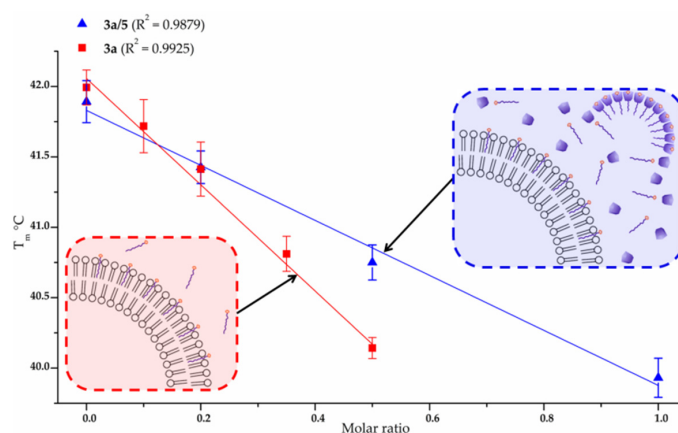


**Figure 7.** Dependences of the lipid phase transition temperature  $T_m$  (DPPC) on the amount of **3a** (red) and systems **3a/5** (blue) at pH = 4.1.

#### 2.4. Interaction of FUDR with Associates **3a/5**

Further, to confirm the hypothesis about the possibility of using systems **3a–d/5** as components of DDS, we investigated the inclusion of the anticancer drug 5-fluoro-2'-deoxyuridine (floxuridine, FUDR) into the structure of the most thermodynamically stable associate (according to DLS data—Table 2) **3a/5** [31]. FUDR is used to treat colorectal, liver and stomach cancers. However, this drug is highly toxic, which causes a large number of side effects such as mouth ulcers, nausea, vomiting, hair loss, stomach ulcers, yellowing of the skin and eyes.

Inclusion of FUDR into associate **3a/5** was studied by DLS,  $^{19}\text{F}$ , 2D DOSY NMR spectroscopy methods. Thus, the study of  $^{19}\text{F}$ -NMR (Figure 8) spectra with proton decoupling FUDR and mixtures **3a/5**/FUDR in the ratios 1:1:1, 1:1:2, 1:1:5, 1:1:7, 1:1:10 ( $1 \times 10^{-3}$  M) was carried out. To prepare studied solutions, FUDR was first dissolved in deionized water,

then meroterpenoid **3a** was added. Then, the solution was thermostated at 25 °C for 10 min and the macrocycle **5** was added.

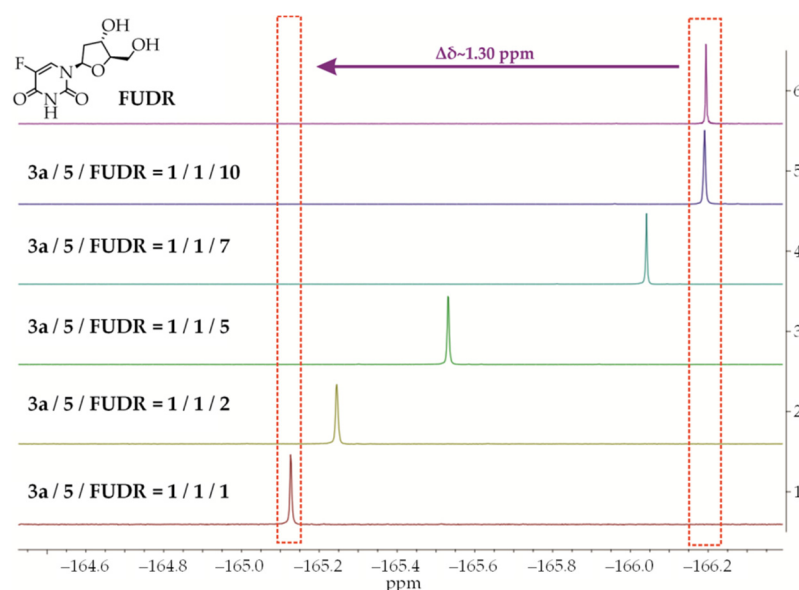


**Figure 8.**  $^{19}\text{F}$ -NMR spectra with proton decoupling ( $1 \times 10^{-3}$  M) in  $\text{D}_2\text{O}$  at 298 K: 1) **3a/5/FUDR** in the ratio 1:1:1; 2) **3a/5/FUDR** in the ratio 1:1:2; 3) **3a/5/FUDR** in the ratio 1:1:5; 4) **3a/5/FUDR** in the ratio 1:1:7; 5) **3a/5/FUDR** in the ratio 1:1:10; 6) FUDR.

In the case of the inclusion of the FUDR molecule in the structure of the supramolecular associate, a shift of the fluorine signal to the weak field of the spectrum is observed [32]. It should be noted that in the case of the **3a/5/FUDR** system in a 1:1:1 ratio ( $1 \times 10^{-3}$  M), a shift of the fluorine signal by  $\Delta\delta \sim 1.30$  ppm is observed (Figure 8) compared to free FUDR. Based on this, we can conclude that the shift of the fluorine signal in **3a/5/FUDR** to the downfield region of the spectrum indicates the inclusion of the FUDR molecule in the structure of the supramolecular associate, as well as the de-shielding of the fluorine atom caused by the presence of fluorine inside the associate **3a/5** [33]. An increase of the concentration of FUDR in the **3a/5/FUDR** system ( $1 \times 10^{-3}$ – $1 \times 10^{-2}$  M) leads to the return of the  $^{19}\text{F}$  signal to its original value. This is apparently associated with saturation of the **3a/5/FUDR** associates and an increase in the concentration of free FUDR. Also, the absence of interaction between FUDR and pillar[5]arene was established by  $^1\text{H}$ - and  $^{19}\text{F}$ -NMR spectroscopy.

DLS studies of the obtained aggregates **3a/5/FUDR** = 1: 1: 1 showed that associates are formed in the entire range of investigated concentrations ( $1 \times 10^{-3}$ – $1 \times 10^{-5}$  M). The most stable **3a/5/FUDR** systems are formed at a concentration of  $1 \times 10^{-4}$  M. Aggregates with an average hydrodynamic diameter of  $299 \pm 10$  nm and a PDI 0.25 are formed. The electrokinetic potential of the resulting systems was  $-78 \pm 3$  mV. In the case of destruction of the **3a/5** systems in the presence of FUDR, the zeta potential values would be closer to zero. Negative value of the zeta potential allows us to conclude that the FUDR is inside the **3a/5** associates.

The formation of **3a/5/FUDR** associates was additionally confirmed by 2D DOSY spectroscopy. Diffusion coefficients of FUDR, **3a/5** and **3a/5/FUDR** at 298 K ( $1 \times 10^{-3}$  M) were determined. The DOSY spectrum of the **3a/5/FUDR** system in a 1:1:1 ratio shows the presence of associate signals lying on one straight line (Figure 9), with one diffusion coefficient ( $D = 4.01 \times 10^{-10} \text{ m}^2\text{s}^{-1}$ ). This is significantly lower than the self-diffusion coefficient of FUDR ( $D = 7.65 \times 10^{-10} \text{ m}^2\text{s}^{-1}$ ) and associates **3a/5** ( $D = 5.12 \times 10^{-10} \text{ m}^2\text{s}^{-1}$ ) under the same conditions. The results obtained unambiguously indicate the incorporation of FUDR into the structure of the supramolecular associate **3a/5**. The results obtained are in good agreement with the literature data [34].

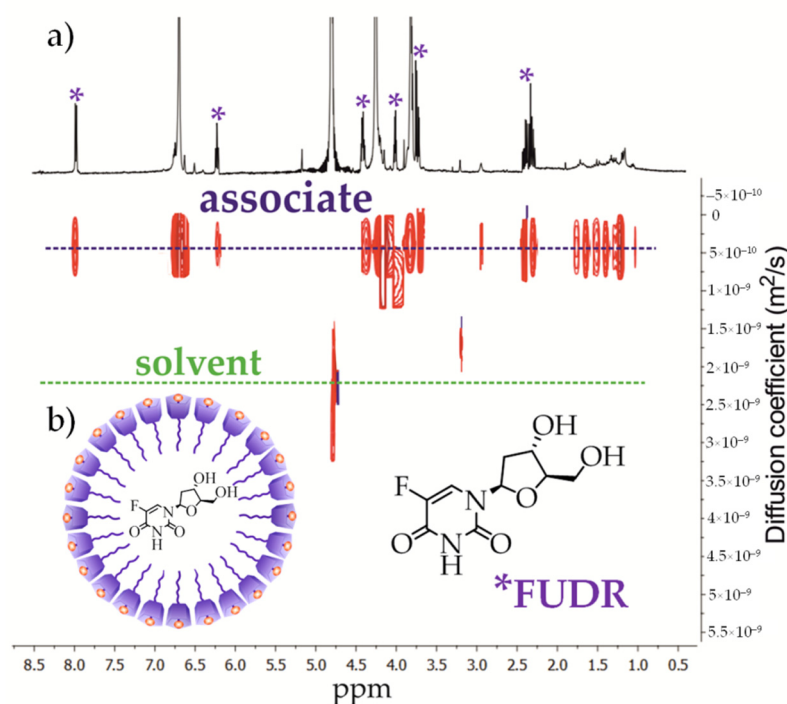


**Figure 9.** (a) 2D DOSY NMR spectrum **3a/5/FUDR** ( $1 \times 10^{-3}$  M) in  $D_2O$  (400 MHz, 298K), 298K, (b) schematic picture of the **3a/5/FUDR** associate.

Thus, a stable self-assembling system of supramolecular amphiphiles based on pillar[5]arene **5** and meroterpenoids **3a–d** was obtained. Systems are able to form associates with FUDR. It was confirmed that FUDR is inside the associate **5/3a–d**. Using a pH-control, it is possible to release FUDR from associates in a targeted manner.

### 3. Experimental

#### 3.1. General Information

All reagents and solvents (Sigma-Aldrich, St. Louis, MO, USA) were used directly as purchased or purified according to the standard procedures. The  $^1H$ -,  $^{13}C$ - and  $^{19}F$ -NMR spectra were recorded on an Avance 400 spectrometer (Bruker Corp., Billerica, MA, USA) (400 MHz for H-atoms) for 3–5% solutions in  $CDCl_3$ ,  $D_2O$ ,  $CD_3OD$ ,  $DMSO-d_6$ . The residual solvent peaks were used as an internal standard. Elemental analysis was performed on a Perkin-Elmer 2400 Series II instrument (Perkin Elmer, Waltham, MA, USA). The FTIR ATR spectra were recorded on the Spectrum 400 FT-IR spectrometer (Perkin Elmer, Seer Green, Lantrisant, UK) with a Diamond KRS-5 attenuated total internal reflectance attachment (resolution  $0.5\text{ cm}^{-1}$ , accumulation of 64 scans, recording time 16 s in the wavelength range  $400\text{--}4000\text{ cm}^{-1}$ ). HRMS mass spectra were obtained on a quadrupole time-of-flight (t, qTOF) AB Sciex Triple TOF 5600 mass spectrometer (AB SCIEX PTE. Ltd., Singapore) using a turbo-ion spray source (nebulizer gas nitrogen, a positive ionization polarity, needle voltage 5500 V). Recording of the spectra was performed in “TOF MS” mode with collision energy 10 eV, de-clustering potentially 100 eV and with a resolution of more than 30,000 full-width half-maximum. Samples with the analyte concentration of  $5\text{ }\mu\text{mol/L}$  were prepared by dissolving the test compounds in the mixture of methanol (HPLC-UV Grade, Darmstadt, Germany). Pillar[5]arene **5** was synthesized according to the literature method [25].

#### 3.2. General Procedure for the Synthesis of Compounds **2a–d**

A solution of 0.02 mol of the appropriate terpene alcohol (geraniol, farnesol, or phytol) and 0.021 mol of DIPEA in 60 mL chloroform was prepared in a 250-mL round-bottom flask equipped with a Claisen adapter. The resulting solution was cooled to  $-5\text{ }^\circ\text{C}$ . The Claisen adapter was fitted with a thermometer and a dropping funnel containing a solution

of 0.021 mol of bromoacetyl bromide in 10 mL of chloroform. This solution was added at such a rate that the temperature did not rise above  $-2\text{ }^{\circ}\text{C}$ . After the addition, the reaction mixture was left for 1 h at room temperature. The resulting reaction mixture was then washed with 5% aqueous  $\text{Na}_2\text{CO}_3$  solution ( $2 \times 50\text{ mL}$ ), then washed with 50 mL of water. The solvent was removed on a rotary evaporator, after which the crude product was purified by column chromatography on silica gel (eluent hexane-propanol-2 20:1).

### 3.2.1. Geranyl-2-bromoacetate (2a)

Pale yellow oil, yield: 4.29 g (78%).  $n_D^{20} = 1.4895$ .  $^1\text{H-NMR}$  ( $\text{CDCl}_3$ ,  $\delta$ , ppm,  $J/\text{Hz}$ ): 1.60 (s, 3H,  $\text{CH}_3$ ), 1.68 (s, 3H,  $\text{CH}_3$ ), 1.71 (s, 3H,  $\text{CH}_3$ ), 2.04–2.11 (m, 4H,  $\text{CH}_2\text{-CH}_2$ ), 3.83 (s, 2H,  $\text{O=C-CH}_2\text{Br}$ ), 4.68 (d, 2H,  $=\text{CH-CH}_2\text{-O}$ ,  $^3J_{\text{HH}} = 7.2$ ), 5.07 (m, 1H,  $=\text{CH}$ ), 5.35 (m, 1H,  $=\text{CH}$ ).  $^{13}\text{C-NMR}$  ( $\text{CDCl}_3$ ,  $\delta$ , ppm): 16.54, 17.71, 25.70, 26.11, 26.22, 39.52, 63.13, 117.36, 123.61, 131.93, 143.58, 167.23. FTIR ATR ( $\nu$ ,  $\text{cm}^{-1}$ ): 2967 ( $\text{CH}_2\text{Br}$ ); 2915 ( $\text{CH}_2$ ); 2856 ( $\text{CH}_3$ ); 1735 ( $\text{C=O}$ ); 1444, 1424, 1408 ( $=\text{CH}$ ); 1376 ( $\text{CH}_3$ ); 1276 ( $\text{C-O-C}$ ); 1204, 1153 ( $\text{C-O-C}$ ); 953, 888, 830 ( $=\text{CH}$ ); 554 ( $\text{CH}_2\text{Br}$ ). Elemental analysis. Calculated for  $\text{C}_{12}\text{H}_{19}\text{BrO}_2$ : C, 52.38; H, 6.96; Br, 29.04. Found: C, 52.13; H, 6.77; Br, 28.90.

### 3.2.2. Farnesyl-2-bromoacetate (2b)

Pale yellow oil, yield: 5.15 g (75%).  $n_D^{20} = 1.4970$ .  $^1\text{H-NMR}$  ( $\text{CDCl}_3$ ,  $\delta$ , ppm,  $J/\text{Hz}$ ): 1.60 (s, 6H,  $\text{CH}_3$ ), 1.68 (s, 3H,  $\text{CH}_3$ ), 1.72 (s, 3H,  $\text{CH}_3$ ), 1.96–2.15 (m, 8H,  $\text{CH}_2\text{-CH}_2$ ), 3.84 (s, 2H,  $\text{O=C-CH}_2\text{Br}$ ), 4.69 (d, 2H,  $=\text{CH-CH}_2\text{-O}$ ,  $^3J_{\text{HH}} = 7.3$ ), 5.09 (m, 2H,  $=\text{CH}$ ), 5.35 (m, 1H,  $=\text{CH}$ ).  $^{13}\text{C-NMR}$  ( $\text{CDCl}_3$ ,  $\delta$ , ppm): 16.04, 16.56, 17.71, 25.72, 26.03, 26.12, 26.58, 26.71, 39.53, 39.70, 39.81, 63.15, 117.36, 123.49, 124.29, 131.37, 135.58, 135.71, 143.62, 167.25. FTIR ATR ( $\nu$ ,  $\text{cm}^{-1}$ ): 2965 ( $\text{CH}_2\text{Br}$ ); 2922 ( $\text{CH}_2$ ); 2856 ( $\text{CH}_3$ ); 1735 ( $\text{C=O}$ ); 1669 ( $\text{C=C}$ ), 1445 ( $=\text{CH}$ ); 1376, 1342 ( $\text{CH}_3$ ); 1276 ( $\text{C-O-C}$ ); 1206, 1154 ( $\text{C-O-C}$ ); 956, 887, 828 ( $=\text{CH}$ ); 553 ( $\text{CH}_2\text{Br}$ ). Elemental analysis. Calculated for  $\text{C}_{17}\text{H}_{27}\text{BrO}_2$ : C, 59.48; H, 7.93; Br, 23.27. Found: C, 59.43; H, 7.97; Br, 22.98.

### 3.2.3. Phytol-2-bromoacetate (2c)

Pale yellow oil, yield: 5.76 g (69%).  $n_D^{20} = 1.4710$ .  $^1\text{H-NMR}$  ( $\text{CDCl}_3$ ,  $\delta$ , ppm,  $J/\text{Hz}$ ): 0.83 (s, 3H,  $\text{CH}_3$ ), 0.85 (br. s, 6H,  $\text{CH}_3$ ), 0.87 (s, 3H,  $\text{CH}_3$ ), 1.04–1.10 (m, 4H,  $\text{CH}_2\text{-CH}_2$ ), 1.12–1.16 (m, 2H,  $\text{CH}_2$ ), 1.21–1.26 (m, 6H,  $\text{CH}_2\text{-CH}_2$ ), 1.28–1.32 (m, 2H,  $\text{CH}_2$ ), 1.34–1.42 (m, 4H,  $\text{CH}_2\text{-CH}_2$ ), 1.48–1.56 (m, 1H,  $\text{CH}$ ), 1.73 (br. s, 3H,  $\text{CH}_3$ ), 2.01 (m, 1H,  $\text{CH}$ ), 2.07 (m, 1H,  $\text{CH}$ ), 3.84 (br s, 2H,  $\text{O=C-CH}_2\text{Br}$ ), 4.67 (m, 2H,  $=\text{CH-CH}_2\text{-O}$ ), 5.35 (m, 1H,  $=\text{CH}$ ).  $^{13}\text{C-NMR}$  ( $\text{CDCl}_3$ ,  $\delta$ , ppm): 16.46, 19.62, 19.69, 19.76, 22.65, 22.74, 23.53, 24.47, 24.82, 25.00, 25.64, 26.06, 26.11, 27.99, 32.38, 32.68, 32.71, 32.72, 32.79, 36.60, 36.70, 36.81, 36.91, 37.31, 37.39, 37.44, 39.38, 39.86, 62.86, 63.19, 117.09, 117.85, 144.14, 144.60, 167.25. FTIR ATR ( $\nu$ ,  $\text{cm}^{-1}$ ): 2952 ( $\text{CH}_2\text{Br}$ ); 2925 ( $\text{CH}_2$ ); 2867 ( $\text{CH}_3$ ); 2847 ( $\text{CH}_2$ ); 1738 ( $\text{C=O}$ ); 1461, 1423 ( $=\text{CH}$ ); 1377, 1366 ( $\text{CH}_3$ ); 1276 ( $\text{C-O-C}$ ); 1208, 1154 ( $\text{C-O-C}$ ); 955, 886, 735 ( $=\text{CH}$ ); 555 ( $\text{CH}_2\text{Br}$ ). Elemental analysis. Calculated for  $\text{C}_{22}\text{H}_{41}\text{BrO}_2$ : C, 63.30; H, 9.90; Br, 19.14. Found: C, 64.13; H, 9.97; Br, 18.98.

### 3.2.4. R-Myrtenyl-2-bromoacetate (2d)

Pale yellow oil, yield: 3.88 g (71%).  $n_D^{20} = 1.5698$ .  $^1\text{H-NMR}$  ( $\text{CDCl}_3$ ,  $\delta$ , ppm,  $J/\text{Hz}$ ): 0.82 (s, 3H,  $\text{CH}_3$ ), 1.18 (d, 1H,  $\text{CH}$ ,  $^3J_{\text{HH}} = 8.7$ ), 1.29 (s, 3H,  $\text{CH}_3$ ), 2.07–2.17 (m, 2H,  $\text{CH}_2$ ), 2.21–2.36 (m, 2H,  $\text{CH}_2$ ), 2.41 (m, 1H,  $\text{CH}$ ), 3.83 (s, 2H,  $\text{O=C-CH}_2\text{Br}$ ), 4.55 (s, 2H,  $=\text{CH-CH}_2\text{-O}$ ), 5.62 (s, 1H,  $=\text{CH}$ ).  $^{13}\text{C-NMR}$  ( $\text{CDCl}_3$ ,  $\delta$ , ppm): 21.14, 26.00, 26.14, 31.34, 31.52, 38.10, 40.64, 43.54, 68.79, 122.74, 142.25, 167.23. FTIR ATR ( $\nu$ ,  $\text{cm}^{-1}$ ): 2986 ( $\text{CH}_2\text{Br}$ ); 2916 ( $\text{CH}_2$ ); 2832 ( $\text{CH}_3$ ); 1735 ( $\text{C=O}$ ); 1469, 1447, 1429 ( $=\text{CH}$ ); 1366 ( $\text{CH}_3$ ); 1272 ( $\text{C-O-C}$ ); 1216, 1204, 1160, 1129 ( $\text{C-O-C}$ ); 1044 ( $\text{C-O-C}$ ); 1007, 963 (cyclobutane moiety vibrations); 887, 801 ( $=\text{CH}$ ); 780 ( $=\text{CH}$ ); 547 ( $\text{CH}_2\text{Br}$ ). Elemental analysis. Calculated for  $\text{C}_{12}\text{H}_{17}\text{BrO}_2$ : C, 52.76; H, 6.27; Br, 29.25. Found: C, 53.17; H, 6.61; Br, 27.74;

### 3.3. General Procedure for the Synthesis of Compounds 3a–d and 4a–d

In a 25 mL round-bottom flask, a solution of 1.5 mmol of terpenyl bromoacetate (**2a–d**) in 12 mL of diethyl ether was prepared. To the resulting solution 1.6 mmol of pyridine or *N*-methylimidazole was added. The reaction mixture was stirred at room temperature (in the case of **3c**, **4b,c** heating under reflux was required) for 36 h. Then diethyl ether was removed on a rotary evaporator. The crude residue was washed with hexane to get rid of the starting reagents, then dried on a rotary evaporator under vacuum.

#### 3.3.1. 1-(2-(Geranyloxy)-2-oxoethyl)pyridinium bromide (**3a**)

Brown resin, yield: 0.46 g (87%). <sup>1</sup>H-NMR (CDCl<sub>3</sub>, δ, ppm, J/Hz): 1.59 (s, 3H, CH<sub>3</sub>), 1.67 (s, 3H, CH<sub>3</sub>), 1.70 (s, 3H, CH<sub>3</sub>), 2.03–2.10 (m, 4H, CH<sub>2</sub>–CH<sub>2</sub>), 4.73 (d, 2H, =CH–CH<sub>2</sub>–O, <sup>3</sup>J<sub>HH</sub> = 7.3), 5.06 (m, 1H, =CH), 5.32 (m, 1H, =CH), 6.24 (s, 2H, O=C–CH<sub>2</sub>N<sup>+</sup>), 8.07 (t, 2H, N<sup>+</sup>=CH<sub>ar</sub>–CH<sub>ar</sub>, <sup>3</sup>J<sub>HH</sub> = 7.4, 6.9), 8.52 (t, 1H, N<sup>+</sup>=CH<sub>ar</sub>–CH<sub>ar</sub>=CH<sub>ar</sub>, <sup>3</sup>J<sub>HH</sub> = 7.8), 9.38 (d, 2H, N<sup>+</sup>=CH<sub>ar</sub>, <sup>3</sup>J<sub>HH</sub> = 6.0). <sup>13</sup>C-NMR (CDCl<sub>3</sub>, δ, ppm): 16.55, 17.74, 25.74, 26.21, 39.52, 57.91, 63.13, 117.36, 123.61, 125.26, 131.93, 140.44, 143.58, 145.51, 171.12. FTIR ATR (ν, cm<sup>−1</sup>): 2972 (CH<sub>3</sub>); 2930, 2901 (CH<sub>2</sub>); 1740 (C=O); 1638 (C=C); 1377 (CH<sub>3</sub>); 1241, 1204 (Pyridine); 1075, 1066, 1058, 1028 (C–O–C); 892 (C=C); 775 (CH<sub>ar</sub>). Elemental analysis. Calculated for C<sub>17</sub>H<sub>24</sub>BrNO<sub>2</sub>. C, 56.99; H, 6.69; Br, 22.36; N, 4.01. Found: C, 57.63; H, 6.83; Br, 22.55; N, 3.95.

#### 3.3.2. 1-(2-(Farnesyloxy)-2-oxoethyl)pyridinium bromide (**3b**)

Brown resin, yield: 0.53 g (84%). <sup>1</sup>H-NMR (CDCl<sub>3</sub>, δ, ppm, J/Hz): 1.59 (s, 6H, CH<sub>3</sub>), 1.68 (s, 6H, CH<sub>3</sub>), 1.92–2.13 (m, 8H, CH<sub>2</sub>–CH<sub>2</sub>), 4.74 (d, 2H, =CH–CH<sub>2</sub>–O, <sup>3</sup>J<sub>HH</sub> = 7.4), 5.08 (m, 2H, =CH), 5.34 (m, 1H, =CH), 6.24 (s, 2H, O=C–CH<sub>2</sub>N<sup>+</sup>), 8.07 (t, 2H, N<sup>+</sup>=CH<sub>ar</sub>–CH<sub>ar</sub>, <sup>3</sup>J<sub>HH</sub> = 7.0), 8.51 (t, 1H, N<sup>+</sup>=CH<sub>ar</sub>–CH<sub>ar</sub>=CH<sub>ar</sub>, <sup>3</sup>J<sub>HH</sub> = 7.8), 9.36 (d, 2H, N<sup>+</sup>=CH<sub>ar</sub>, <sup>3</sup>J<sub>HH</sub> = 6.0). <sup>13</sup>C-NMR (CDCl<sub>3</sub>, δ, ppm): 16.01, 16.51, 17.69, 25.74, 26.13, 26.14, 26.61, 39.53, 39.70, 39.81, 58.17, 63.15, 117.33, 123.51, 124.32, 125.29, 131.34, 135.62, 135.69, 140.11, 143.58, 145.49, 167.23. FTIR ATR (ν, cm<sup>−1</sup>): 2969 (CH<sub>3</sub>); 2927 (CH<sub>2</sub>); 1743, 1713 (C=O); 1637 (C=C); 1445 (=CH); 1376 (CH<sub>3</sub>); 1200 (Pyridine); 1076, 1057, 1027 (C–O–C); 775 (CH<sub>ar</sub>). Elemental analysis. Calculated for C<sub>22</sub>H<sub>32</sub>BrNO<sub>2</sub>. C, 63.17; H, 7.72; Br, 18.32; N, 3.41. Found: C, 62.56; H, 7.64; Br, 18.92; N, 3.32.

#### 3.3.3. 1-(2-(Phytyloxy)-2-oxoethyl)pyridinium bromide (**3c**)

Pale brown resin, yield: 0.62 g (73%). <sup>1</sup>H-NMR (CDCl<sub>3</sub>, δ, ppm, J/Hz): 0.83 (br. s, 3H, CH<sub>3</sub>), 0.85 (br. s, 6H, CH<sub>3</sub>), 0.87 (s, 3H, CH<sub>3</sub>), 1.04–1.10 (m, 4H, CH<sub>2</sub>–CH<sub>2</sub>), 1.11–1.14 (m, 2H, CH<sub>2</sub>), 1.20–1.25 (m, 6H, CH<sub>2</sub>–CH<sub>2</sub>), 1.26–1.30 (m, 2H, CH<sub>2</sub>), 1.34–1.42 (m, 4H, CH<sub>2</sub>–CH<sub>2</sub>), 1.47–1.55 (m, 1H, CH), 1.72 (br. s, 3H, CH<sub>3</sub>), 2.02–2.10 (m, 2H, CH), 4.73 (m, 2H, =CH–CH<sub>2</sub>–O), 5.32 (m, 1H, =CH), 6.28 (s, 2H, O=C–CH<sub>2</sub>N<sup>+</sup>), 8.06 (t, 2H, N<sup>+</sup>=CH<sub>ar</sub>–CH<sub>ar</sub>, <sup>3</sup>J<sub>HH</sub> = 7.0), 8.50 (t, 1H, N<sup>+</sup>=CH<sub>ar</sub>–CH<sub>ar</sub>=CH<sub>ar</sub>, <sup>3</sup>J<sub>HH</sub> = 7.7), 9.39 (d, 2H, N<sup>+</sup>=CH<sub>ar</sub>, <sup>3</sup>J<sub>HH</sub> = 6.0). <sup>13</sup>C-NMR (CDCl<sub>3</sub>, δ, ppm): 16.47, 19.67, 19.72, 19.78, 22.69, 22.75, 23.58, 24.50, 25.01, 25.02, 25.69, 26.12, 26.19, 32.40, 32.71, 32.73, 32.76, 32.80, 36.62, 36.72, 36.84, 36.93, 37.32, 37.41, 37.47, 39.41, 39.90, 57.91, 62.88, 63.21, 117.11, 117.91, 125.77, 140.88, 144.20, 144.62, 145.90, 169.13. FTIR ATR (ν, cm<sup>−1</sup>): 2952 (CH<sub>3</sub>); 2924, 2901 (CH<sub>2</sub>); 1737, 1734 (C=O); 1491 (=CH); 1378 (CH<sub>3</sub>); 1207 (Pyridine); 1195, 1058 (C–O–C); 777 (CH<sub>ar</sub>). HRMS: calculated [M – Br]<sup>+</sup> m/z = 416.3524, found: [M – Br]<sup>+</sup> m/z = 416.3487.

#### 3.3.4. 1-(2-(R-Myrtenyloxy)-2-oxoethyl)pyridinium bromide (**3d**)

Yellow resin, yield: 0.4 g (75%). <sup>1</sup>H-NMR (CDCl<sub>3</sub>, δ, ppm, J/Hz): 0.77 (s, 3H, CH<sub>3</sub>), 1.13 (d, 1H, CH, <sup>3</sup>J<sub>HH</sub> = 8.6), 1.29 (s, 3H, CH<sub>3</sub>), 2.07–2.14 (m, 2H, CH<sub>2</sub>), 2.20–2.36 (m, 2H, CH<sub>2</sub>), 2.41 (m, 1H, CH), 4.58 (s, 2H, CH<sub>2</sub>–O), 5.62 (s, 1H, =CH), 6.25 (m, 2H, O=C–CH<sub>2</sub>N<sup>+</sup>), 8.07 (t, 2H, N<sup>+</sup>=CH<sub>ar</sub>–CH<sub>ar</sub>, <sup>3</sup>J<sub>HH</sub> = 6.9), 8.51 (t, 1H, N<sup>+</sup>=CH<sub>ar</sub>–CH<sub>ar</sub>=CH<sub>ar</sub>, <sup>3</sup>J<sub>HH</sub> = 8.0), 9.37 (d, 2H, N<sup>+</sup>=CH<sub>ar</sub>, <sup>3</sup>J<sub>HH</sub> = 6.0). <sup>13</sup>C-NMR (DMSO-d<sub>6</sub>, δ, ppm): 21.50, 26.49, 32.24, 32.35, 38.95, 41.87, 44.66, 61.87, 70.38, 124.15, 129.11, 129.23, 143.38, 147.58, 148.08, 167.08. FTIR ATR (ν, cm<sup>−1</sup>): 3039, 3017 (C–H); 2989 (CH<sub>3</sub>); 2916, 2882, 2830 (CH<sub>2</sub>); 1749 (C=O); 1638,

1502 (C=N<sub>pyridine</sub>); 1468 (CH<sub>3</sub>); 1444, 1430 (=C-H); 1368 (CH<sub>3</sub>); 1267 (C-O-C); 1243, 1160, 1131 (C-O-C); 950 (cyclobutane moiety vibrations); 785, 774 (=CH); 671 (=CH). HRMS: calculated [M - Br<sup>-</sup>]<sup>+</sup> *m/z* = 272.1645, found: [M - Br<sup>-</sup>]<sup>+</sup> *m/z* = 272.1651.

### 3.3.5. 3-(2-(Geranyloxy)-2-oxoethyl)-1-methyl-1H-imidazole-3-ium bromide (4a)

Yellow resin, yield: 0.44 g (83%). <sup>1</sup>H-NMR (CDCl<sub>3</sub>, δ, ppm, *J*/Hz): 1.59 (s, 3H, CH<sub>3</sub>), 1.67 (s, 3H, CH<sub>3</sub>), 1.70 (s, 3H, CH<sub>3</sub>), 2.03–2.10 (m, 4H, CH<sub>2</sub>-CH<sub>2</sub>), 4.07 (s, 3H, CH<sub>3</sub>N), 4.71 (d, 2H, =CH-CH<sub>2</sub>-O, <sup>3</sup>*J*<sub>HH</sub> = 7.3), 5.05 (m, 1H, =CH), 5.32 (m, 1H, =CH), 5.43 (s, 2H, O=C-CH<sub>2</sub>N<sup>+</sup>), 7.41 (s, 1H, CH<sub>imidazole</sub>), 7.52 (s, 1H, CH<sub>imidazole</sub>), 10.21 (s, 1H, CH<sub>imidazole</sub>). <sup>13</sup>C-NMR (CDCl<sub>3</sub>, δ, ppm): 16.66, 17.80, 25.77, 26.27, 36.99, 39.60, 59.34, 63.73, 116.91, 123.12, 123.60, 123.77, 132.06, 138.45, 144.28, 166.19. FTIR ATR (*ν*, cm<sup>-1</sup>): 3401, 3154, 3098 (=C-H); 2966 (CH<sub>3</sub>); 2915, 2856 (CH<sub>2</sub>); 1623 (C=O); (C=C); 1577 (C=N<sub>imidazole</sub>); 1437 (CH<sub>2</sub>CO); 1381, 1345 (CH<sub>3</sub>); 1215, 1196, 1173 (C-O-C); 1104 (C-O-C); 1035 (C=N<sub>imidazole</sub>); 975, 941, 892 (=C-H); 775, 753, 756 (CH<sub>imidazole</sub>). Elemental analysis. Calculated for C<sub>21</sub>H<sub>33</sub>BrN<sub>2</sub>O<sub>2</sub>. C, 53.79; H, 7.05; Br, 22.36; N, 7.84. Found: C, 53.81; H, 7.09; Br, 22.29; N, 7.81.

### 3.3.6. 3-(2-(Farnesyloxy)-2-oxoethyl)-1-methyl-1H-imidazole-3-ium bromide (4b)

Yellow resin, yield: 0.52 g (81%). <sup>1</sup>H-NMR (CDCl<sub>3</sub>, δ, ppm, *J*/Hz): 1.60 (s, 6H, CH<sub>3</sub>), 1.68 (s, 3H, CH<sub>3</sub>), 1.72 (s, 3H, CH<sub>3</sub>), 1.95–2.11 (m, 8H, CH<sub>2</sub>-CH<sub>2</sub>), 4.08 (s, 3H, CH<sub>3</sub>N), 4.73 (d, 2H, =CH-CH<sub>2</sub>-O, <sup>3</sup>*J*<sub>HH</sub> = 7.5), 5.08 (t, 2H, =CH, <sup>3</sup>*J*<sub>HH</sub> = 6.4), 5.34 (t, 1H, =CH, <sup>3</sup>*J*<sub>HH</sub> = 6.9), 5.43 (s, 2H, O=C-CH<sub>2</sub>N<sup>+</sup>), 7.29 (s, 1H, CH<sub>imidazole</sub>), 7.42 (s, 1H, CH<sub>imidazole</sub>), 10.52 (s, 1H, CH<sub>imidazole</sub>). <sup>13</sup>C-NMR (CDCl<sub>3</sub>, δ, ppm): 16.63, 19.30, 24.57, 27.07, 33.16, 37.12, 39.65, 50.17, 61.62, 119.87, 124.65, 131.65, 134.83, 140.55, 165.26. FTIR ATR (*ν*, cm<sup>-1</sup>): 2966 (CH<sub>3</sub>); 2915 (CH<sub>2</sub>); 1746 (C=O); 1437 (CH<sub>2</sub>CO); 1382, 1377, 1365 (CH<sub>3</sub>); 1271, 1215, 1197, 1173 (C-O-C); 973, 941 (=C-H); 732, 703, 621 (CH<sub>imidazole</sub>). Elemental analysis. Calculated for C<sub>21</sub>H<sub>33</sub>BrN<sub>2</sub>O<sub>2</sub>. C, 59.29; H, 7.82; Br, 18.78; N, 6.59. Found: C, 59.30; H, 7.79; Br, 18.89; N, 6.52.

### 3.3.7. 3-(2-(Phytoloxo)-2-oxoethyl)-1-methyl-1H-imidazole-3-ium bromide (4c)

Yellow resin, yield: 0.58 g (78%). <sup>1</sup>H-NMR (CDCl<sub>3</sub>, δ, ppm, *J*/Hz): 0.82 (br. s, 3H, CH<sub>3</sub>), 0.84 (br. s, 6H, CH<sub>3</sub>), 0.86 (s, 3H, CH<sub>3</sub>), 1.02–1.08 (m, 4H, CH<sub>2</sub>-CH<sub>2</sub>), 1.10–1.14 (m, 2H, CH<sub>2</sub>), 1.19–1.24 (m, 6H, CH<sub>2</sub>-CH<sub>2</sub>), 1.26–1.29 (m, 2H, CH<sub>2</sub>), 1.32–1.40 (m, 4H, CH<sub>2</sub>-CH<sub>2</sub>), 1.46–1.53 (m, 1H, CH), 1.72 (br. s, 3H, CH<sub>3</sub>), 1.98–2.08 (m, 2H, CH), 4.08 (s, 3H, CH<sub>3</sub>N), 4.71 (m, 2H, =CH-CH<sub>2</sub>-O), 5.32 (m, 1H, =CH), 5.42 (s, 2H, O=C-CH<sub>2</sub>N<sup>+</sup>), 7.36 (s, 1H, CH<sub>imidazole</sub>), 7.47 (s, 1H, CH<sub>imidazole</sub>), 10.29 (s, 1H, CH<sub>imidazole</sub>). <sup>13</sup>C-NMR (CDCl<sub>3</sub>, δ, ppm): 15.19, 18.44, 18.48, 18.55, 21.43, 21.53, 22.26, 23.36, 23.63, 24.16, 26.54, 30.95, 31.21, 31.29, 35.21, 35.92, 37.93, 48.63, 49.11, 61.50, 61.84, 115.71, 116.67, 122.07, 122.83, 136.68, 142.70, 165.18, 166.67. FTIR ATR (*ν*, cm<sup>-1</sup>): 2952 (CH<sub>3</sub>); 2925, 2868 (CH<sub>2</sub>); 1747 (C=O); 1577, 1566 (C=N<sub>imidazole</sub>); 1462 (=CH); 1377, 1366 (CH<sub>3</sub>); 1218 (Imidazole); 1199, 1174 (C-O-C); 942, 621 (CH<sub>imidazole</sub>). HRMS: calculated [M - Br<sup>-</sup>]<sup>+</sup> *m/z* = 419.3632, found [M - Br<sup>-</sup>]<sup>+</sup> *m/z* = 419.3638.

### 3.3.8. 3-(2-(R-Myrtenyloxy)-2-oxoethyl)-1-methyl-1H-imidazole-3-ium bromide (4d)

Yellow resin, yield: 0.45 g (84%). <sup>1</sup>H-NMR (CDCl<sub>3</sub>, δ, ppm, *J*/Hz): 0.79 (s, 3H, CH<sub>3</sub>), 1.15 (d, 1H, CH, <sup>3</sup>*J*<sub>HH</sub> = 8.8), 1.29 (s, 3H, CH<sub>3</sub>), 2.10–2.15 (m, 2H, CH<sub>2</sub>), 2.22–2.34 (m, 2H, CH<sub>2</sub>), 2.41 (m, 1H, CH), 4.07 (s, 3H, CH<sub>3</sub>N), 4.57 (s, 2H, CH<sub>2</sub>-O), 5.43 (m, 2H, O=C-CH<sub>2</sub>N<sup>+</sup>), 5.62 (s, 1H, =CH), 7.35 (s, 1H, CH<sub>imidazole</sub>), 7.44 (s, 1H, CH<sub>imidazole</sub>), 10.30 (s, 1H, CH<sub>imidazole</sub>). <sup>13</sup>C NMR (CDCl<sub>3</sub>, δ, ppm): 21.05, 26.02, 31.23, 31.43, 36.91, 37.99, 40.45, 43.39, 50.23, 69.33, 123.29, 123.36, 123.77, 138.12, 141.47, 165.97. FTIR ATR (*ν*, cm<sup>-1</sup>): 3409, 3147, 3067 (=C-H); 2986 (CH<sub>3</sub>); 2914, 2831 (CH<sub>2</sub>); 1747 (C=O); 1627, 1576, (C=N<sub>imidazole</sub>); 1467 (CH<sub>3</sub>); 1430 (=C-H); 1382, 1341 (CH<sub>3</sub>); 1265 (C-O-C); 1171 (C-O-C); 952 (cyclobutane moiety vibrations); 795, 776 (=CH); 697 (=CH). HRMS: calculated [M - Br<sup>-</sup>]<sup>+</sup> *m/z* = 275.1754, found: [M - Br<sup>-</sup>]<sup>+</sup> *m/z* = 275.1760.

### 3.4. Determination of the Hydrodynamic Particle Size by Dynamic Light Scattering

The particle size distribution was determined by dynamic light scattering on a Zetasizer Nano ZS nanoparticle size analyzer (Malvern, Worcestershire, UK) in quartz cuvettes. The instrument is equipped with a 4 mW He-Ne laser operating at 633 nm. The measurements were carried out at a measurement angle of  $173^\circ$ , and the measurement position inside the cuvettes was determined automatically. The results were processed using the DTS program (Dispersion Technology Software 4.20). To prepare solutions, deionized water with a resistance of  $18.0 \text{ M}\Omega\cdot\text{cm}$ , obtained using a Millipore-Q purification system, or methanol (HPLC-UV Grade, Darmstadt, Germany) were used. During the experiment, the concentrations of compounds varied from  $1 \times 10^{-5}$  to  $1 \times 10^{-3} \text{ M}$ .

### 3.5. Measurement of the Zeta-Potential

The electrokinetic potential of aggregates compounds was measured on a Zetasizer Nano ZS instrument at  $25^\circ\text{C}$ . The device is equipped with a 4 mW He-Ne laser operating at 633 nm and includes non-invasive backscatter optics. The measurements were carried out at a detection angle of  $173^\circ$ , and the position of the measurement in the cuvette was automatically determined by the software. The results were processed using the DTS package (Dispersion Technology Software 4.20).

### 3.6. Turbidimetry

Experiments to determine the temperature of the phase transition were carried out by measuring the turbidity of a dilute lipid suspension (0.7 mM) on a UV-3600 spectrophotometer (Shimadzu, Kyoto, Japan) equipped with Peltier temperature control unit, the thickness of the transmission layer was 1 cm, the slit width was 1 nm, and the wavelength was 400 nm. Titration of the lipid by the test compounds was carried out in quartz cells. To reduce the experimental error, the obtained compounds were added to 3 mL of a lipid suspension (0.7 mmol) as their concentrated solutions into a buffer 7.4 (50 mM Tris-HCl, 150 mM NaCl, pH 7.4) or buffer 4.1 (50 mM AcOH, pH 4.1). To determine the temperature of the lipid phase transition, we measured the optical density of the samples in the temperature range  $38\text{--}43^\circ\text{C}$  in steps of  $0.1^\circ\text{C}$  per minute. Experimental data on the dependence of the optical density of the emulsion of the vesicles were mathematically processed in the software package Origin 8.1 (OriginLab Corporation, Northampton, MA, USA) by the Van-Hoff 2-state model giving the phase transition temperature ( $T_m$ ) of the system [28].

### 3.7. 2D DOSY NMR Spectroscopy

$^1\text{H}$  diffusion ordered spectroscopy (DOSY) spectra were recorded on a Bruker Avance 400 spectrometer at 9.4 Tesla at a resonating frequency of 400.17 MHz for  $^1\text{H}$  using a BBO Bruker 5 mm gradient probe. The temperature was regulated at 298 K and no spinning was applied to the NMR tube. DOSY experiments were performed using the STE bipolar gradient pulse pair (stebpgp1s) pulse sequence with 16 scans of 16 data points collected. The maximum gradient strength produced in the z direction was  $5.35 \text{ Gmm}^{-1}$ . The duration of the magnetic field pulse gradients ( $\delta$ ) was optimized for each diffusion time ( $\Delta$ ) in order to obtain a 2% residual signal with the maximum gradient strength. The values of  $\delta$  and  $\Delta$  were  $1.800 \mu\text{s}$  and 100 ms, respectively. The pulse gradients were incremented from 2 to 95% of the maximum gradient strength in a linear ramp [35].

## 4. Conclusions

For the first time and using an original methodology, meroterpenoids containing hydrophilic pyridine **3a–d** and imidazole fragments **4a–d**, as well as hydrophobic terpene residues of geraniol, myrtenol, farnesol, and phytol were synthesized. The ability of the water-soluble pillar[5]arene **5** containing carboxylate fragments to form supramolecular amphiphiles by the principle of the formation of host-guest complexes with synthesized meroterpenoids containing pyridine fragments **3a–d** was shown. The association constants of the complexes were determined by UV-vis spectroscopy:  $K_{\text{ass}}(\mathbf{3a/5}) = 8557 \text{ M}^{-1}$  and  $K_{\text{ass}}$

(3b/5) = 14900 M<sup>-1</sup>. Analysis of the binding isotherms obtained using the BindFit software showed that the stoichiometry of the 5/meroterpenoid was 1:1. It was shown by dynamic light scattering that supramolecular amphiphiles 3a–d/5 form monodisperse associates in a wide concentration range ( $1 \times 10^{-3}$ – $1 \times 10^{-5}$  M). 3a/5 systems do not interact with the DPPC model cell membrane at pH 7.4, but the associate is destroyed with a change in pH (pH 4.1) according to turbidimetry data. Upon the destruction of the associate, the initial meroterpenoid 3a is released and embedded into the DPPC lipid bilayer. Using the methods of dynamic light scattering, <sup>19</sup>F, 2D DOSY NMR spectroscopy, the incorporation of the antitumor drug 5-fluoro-2'-deoxyuridine (floxuridine) into the structure of the supramolecular associate 3a/5 was shown. DLS studies of the obtained 3a/5/Floxuridine aggregates with a composition of 1:1:1 ( $1 \times 10^{-3}$ M) showed that associates are formed in the entire range of investigated concentrations ( $1 \times 10^{-3}$ – $1 \times 10^{-5}$  M). The most stable 3a/5/Floxuridine systems are formed at a concentration of  $1 \times 10^{-4}$  M. Aggregates with an average hydrodynamic diameter of  $299 \pm 10$  nm and a PDI of 0.25 are formed. The electrokinetic potential of the obtained systems was  $-78 \pm 3$  mV, which indicates that the floxuridine is inside the 3a/5. The results obtained may find application in the creation of a new generation of non-toxic biomimetic delivery systems for anticancer drugs.

**Supplementary Materials:** The following are available online at <https://www.mdpi.com/article/10.3390/ijms22157950/s1>.

**Author Contributions:** Conceptualization, writing—review and editing, supervision, I.I.S., D.N.S. and V.V.P.; investigation, writing—original draft preparation A.A.A.; funding acquisition, A.A.A., A.I.K. and P.L.P.; investigation and methodology A.A.A., P.L.P., A.I.K., R.R.G., Y.V.P., A.F.G., D.Y.G. All authors have read and agreed to the published version of the manuscript.

**Funding:** The reported study was funded by RFBR, project number 19-33-90170 and project number 19-33-90092.

**Data Availability Statement:** The data presented in this study are available in Supplementary Materials.

**Acknowledgments:** The investigation of spatial structure of the compounds by NMR spectroscopy was carried out within the framework of the grant of the President of the Russian Federation for state support of leading scientific schools of Russian Federation (NSh-2499.2020.3). P.L.P. and D.N.S. acknowledges funding by the subsidy allocated to Kazan Federal University for the state assignment in the sphere of scientific activities (grant No 0671–2020–0063).

**Conflicts of Interest:** The authors declare no conflict of interest. The funders had no role in the design of the study; in the collection, analyses, or interpretation of data; in the writing of the manuscript, or in the decision to publish the results.

## References

1. Kim, S.K. (Ed.) *Handbook of Anticancer Drugs from Marine Origin*; Springer: Berlin, Germany, 2014. [CrossRef]
2. Matsuda, Y.; Abe, I. Biosynthesis of fungal meroterpenoids. *Nat. Prod. Rep.* **2016**, *33*, 26–53. [CrossRef] [PubMed]
3. Plemenkov, V.V.; Shurpik, D.N.; Akhmedov, A.A.; Pupilampu, J.B.; Stoikov, I.I. Progress in studies on meroterpenoids. In *Studies in Natural Products Chemistry*; Ur-Rahman, A., Ed.; Elsevier: Amsterdam, The Netherlands, 2020; Volume 64, pp. 181–216. [CrossRef]
4. Shurpik, D.N.; Akhmedov, A.A.; Cragg, P.J.; Plemenkov, V.V.; Stoikov, I.I. Progress in the Chemistry of Macrocyclic Meroterpenoids. *Plants* **2020**, *9*, 1582. [CrossRef]
5. Woese, C.R.; Kandler, O.; Wheelis, M.L. Towards a natural system of organisms: Proposal for the domains Archaea, Bacteria, and Eucarya. *Proc. Natl. Acad. Sci. USA* **1990**, *87*, 4576–4579. [CrossRef]
6. Caforio, A.; Jain, S.; Fodran, P.; Siliakus, M.; Minnaard, A.J.; Van Der Oost, J.; Driessen, A.J. Formation of the ether lipids archaetidylglycerol and archaetidylethanolamine in *Escherichia coli*. *Biochem. J.* **2015**, *470*, 343–355. [CrossRef] [PubMed]
7. Jain, S.; Caforio, A.; Driessen, A.J.M. Biosynthesis of archaeal membrane ether lipids. *Front. Microbiol.* **2014**, *5*, 641. [CrossRef]
8. Benvegnu, T.; Lemiègre, L.; Cammas-Marion, S. New generation of liposomes called archaeosomes based on natural or synthetic archaeal lipids as innovative formulations for drug delivery. *Recent. Pat. Drug. Deliv. Form.* **2009**, *3*, 206–220. [CrossRef] [PubMed]
9. Jacquemet, A.; Barbeau, J.; Lemiègre, L.; Benvegnu, T. Archaeal tetraether bipolar lipids: Structures, functions and applications. *Biochimica* **2009**, *91*, 711–717. [CrossRef] [PubMed]
10. Akhmedov, A.A.; Shurpik, D.N.; Plemenkov, V.V.; Stoikov, I.I. Water-soluble meroterpenes containing an aminoglyceride fragment with geraniol residues: Synthesis and membranotropic properties. *Mendeleev Commun.* **2019**, *29*, 29–31. [CrossRef]

11. Koga, Y.; Morii, H. Recent Advances in Structural Research on Ether Lipids from Archaea Including Comparative and Physiological Aspects. *Biosci. Biotechnol. Biochem.* **2005**, *69*, 2019–2034. [[CrossRef](#)] [[PubMed](#)]
12. Yan, T.; Li, F.; Tian, J.; Wang, L.; Luo, Q.; Hou, C.; Dong, Z.; Xu, J.; Liu, J. Biomimetic pulsating vesicles with both pH-tunable membrane permeability and light-triggered disassembly–re-assembly behaviors prepared by supra-amphiphilic helices. *ACS Appl. Mater. Interfaces* **2019**, *11*, 30566–30574. [[CrossRef](#)]
13. Shurpik, D.N.; Sevastyanov, D.A.; Zelenikhin, P.V.; Subakaeva, E.V.; Evtugyn, V.G.; Osin, Y.N.; Cragg, P.J.; Stoikov, I.I. Hydrazides of glycine-containing decasubstituted pillar [5] arenes: Synthesis and encapsulation of Floxuridine. *Tetrahedron Lett.* **2018**, *59*, 4410–4415. [[CrossRef](#)]
14. Shurpik, D.N.; Mostovaya, O.A.; Sevastyanov, D.A.; Lenina, O.A.; Sapunova, A.S.; Voloshina, A.D.; Petrov, K.A.; Kovyazina, I.V.; Cragg, P.J.; Stoikov, I.I. Supramolecular neuromuscular blocker inhibition by a pillar[5]arene through aqueous inclusion of rocuronium bromide. *Org. Biomol. Chem.* **2019**, *17*, 9951–9959. [[CrossRef](#)]
15. Li, Z.; Yang, Y.-W. Functional Materials with Pillarene Struts. *Accounts Mater. Res.* **2021**, *2*, 292–305. [[CrossRef](#)]
16. Fa, S.; Kakuta, T.; Yamagishi, T.-A.; Ogoshi, T. One-, Two-, and Three-Dimensional Supramolecular Assemblies Based on Tubular and Regular Polygonal Structures of Pillar[n]arenes. *CCS Chem.* **2019**, *1*, 50–63. [[CrossRef](#)]
17. Ogoshi, T.; Kanai, S.; Fujinami, S.; Yamagishi, T.A.; Nakamoto, Y. para-Bridged symmetrical pillar[5]arenes: Their Lewis acid catalyzed synthesis and host-guest property. *J. Am. Chem. Soc.* **2008**, *130*, 5022–5023. [[CrossRef](#)] [[PubMed](#)]
18. Ogoshi, T.; Tanaka, S.; Yamagishi, T.-A.; Nakamoto, Y. Ionic Liquid Molecules (ILs) as Novel Guests for Pillar[5]arene: 1:2 Host-Guest Complexes between Pillar[5]arene and ILs in Organic Media. *Chem. Lett.* **2011**, *40*, 96–98. [[CrossRef](#)]
19. Cao, D.; Meier, H. Pillar[n]arenes—a Novel, Highly Promising Class of Macrocyclic Host Molecules. *Asian J. Org. Chem.* **2014**, *3*, 244–262. [[CrossRef](#)]
20. Ogoshi, T.; Masaki, K.; Shiga, R.; Kitajima, K.; Yamagishi, T.-A. Planar-Chiral Macrocyclic Host Pillar[5]arene: No Rotation of Units and Isolation of Enantiomers by Introducing Bulky Substituents. *Org. Lett.* **2011**, *13*, 1264–1266. [[CrossRef](#)]
21. Ogoshi, T.; Hashizume, M.; Yamagishi, T.-A.; Nakamoto, Y. Synthesis, conformational and host-guest properties of water-soluble pillar[5]arene. *Chem. Commun.* **2010**, *46*, 3708–3710. [[CrossRef](#)] [[PubMed](#)]
22. Beneteau, R.; Lebreton, J.; Denes, F. A Convenient Access to  $\gamma$ -Lactones from O-Allyl- $\alpha$ -Bromoesters using a One-Pot Ionic-Radical-Ionic Sequence. *Chem. Asian J.* **2012**, *7*, 1516–1520. [[CrossRef](#)]
23. Bhadani, A.; Rane, J.; Veresmortean, C.; Banerjee, S.; John, G. Bio-inspired surfactants capable of generating plant volatiles. *Soft Matter* **2015**, *11*, 3076–3082. [[CrossRef](#)]
24. Hardy, F.E.; Struillou, A.P. Betaine esters for delivery of alcohols. WO Patent 1996038528A1, 13 May 1996. and issued 5 December 1996.
25. Li, C.; Shu, X.; Li, J.; Chen, S.; Han, K.; Xu, M.; Hu, B.; Yu, Y.; Jia, X. Complexation of 1,4-Bis(pyridinium)butanes by Negatively Charged Carboxylatopillar[5]arene. *J. Org. Chem.* **2011**, *76*, 8458–8465. [[CrossRef](#)]
26. Li, C.; Xu, Q.; Li, J.; Yao, F.; Jia, X. Complex interactions of pillar[5]arene with paraquats and bis(pyridinium) derivatives. *Org. Biomol. Chem.* **2010**, *8*, 1568–1576. [[CrossRef](#)] [[PubMed](#)]
27. Hibbert, D.B.; Thordarson, P. The death of the Job plot, transparency, open science and online tools, uncertainty estimation methods and other developments in supramolecular chemistry data analysis. *Chem. Commun.* **2016**, *52*, 12792–12805. [[CrossRef](#)]
28. Eker, F.; Durmus, H.O.; Akinoglu, B.G.; Severcan, F. Application of turbidity technique on peptide-lipid and drug-lipid interactions. *J. Mol. Struct.* **1999**, *482–483*, 693–697. [[CrossRef](#)]
29. Zhang, X.; Lin, Y.; Gillies, R.J. Tumor pH and Its Measurement. *J. Nucl. Med.* **2010**, *51*, 1167–1170. [[CrossRef](#)]
30. Engin, K.; Leeper, D.B.; Cater, J.R.; Thistlethwaite, A.J.; Tupchong, L.; McFarlane, J.D. Extracellular pH distribution in human tumours. *Int. J. Hyperth.* **1995**, *11*, 211–216. [[CrossRef](#)]
31. Grem, J.L. 5-Fluorouracil: Forty-Plus and Still Ticking. A Review of its Preclinical and Clinical Development. *Investig. New Drugs* **2000**, *18*, 299–313. [[CrossRef](#)]
32. Guo, W.; Fung, B.M.; Christian, S.D. NMR study of cyclodextrin inclusion of fluorocarbon surfactants in solution. *Langmuir* **1992**, *8*, 446–451. [[CrossRef](#)]
33. Weiss-Errico, M.J.; Ghiviriga, I.; O’Shea, K.E. <sup>19</sup>F NMR characterization of the encapsulation of emerging perfluoroethercarboxylic acids by cyclodextrins. *J. Phys. Chem. B* **2017**, *121*, 8359–8366. [[CrossRef](#)]
34. Notti, A.; Pisagatti, I.; Nastasi, F.; Patanè, S.; Parisi, M.F.; Gattuso, G. Stimuli-Responsive Internally Ion-Paired Supramolecular Polymer Based on a Bis-pillar[5]arene Dicarboxylic Acid Monomer. *J. Org. Chem.* **2021**, *86*, 1676–1684. [[CrossRef](#)] [[PubMed](#)]
35. Dais, P.; Misiak, M.; Hatzakis, E. Analysis of marine dietary supplements using NMR spectroscopy. *Anal. Methods* **2015**, *7*, 5226–5238. [[CrossRef](#)]